Double common-path interferometer for flexible optical probe of optical coherence tomography

Jae Seok Park[1], **Zhongping Chen**[1,2], **Myung Yung Jeong**[1], and **Chang-Seok Kim**[1,*]

[1]Department of Cogno Mechatronics Engineering, World Class University Program, Pusan National University, Busan 609-735, South Korea

[2]Beckman Laser Institute, Department of Biomedical Engineering, University of California, Irvine, California 92612, USA

Abstract

A flexible curled optical cord is useful for a common-path optical coherence tomography (OCT) system because a bending-insensitive arbitrary length can be chosen for the endoscopic imaging probe. However, there has been a critical problem that the partial reflector needs to be placed in between the sample and the objective lens. It limits the structure design of optical probe and leads to a low transverse resolution OCT imaging. Instead of a conventional single common-path interferometer, we propose a novel double common-path interferometer configuration in order to generate an interference signal that is independent of the optical distance between the partial reflector and sample. Due to the limitless tuning of the objective distance, an objective lens with a high numerical aperture (NA) up to 0.85 can be successfully used for phase-sensitive optical coherence tomography to achieve a 3-dimensional profile image of a transverse resolution of 0.7 μm. The intensity and phase terms of the interference signal can be obtained simultaneously from a Fourier-domain mode locked swept laser source for fast data acquisition with a phase stability of 979 pm.

1. Introduction

Optical coherence tomography (OCT) is useful for various sensing applications, including medical imaging diagnostics as well as industrial surface profilometry [1, 2]. A flexible optical probe is one of the key components of the OCT system, delivering the reflected optical signal from the sample to the imaging system at a remote location. We have suggested a curled optical cord based on a holey fiber to be used as a bending-insensitive arbitrary-length optical imaging probe for a common-path OCT system [3]. However, there has been a critical problem with this common-path OCT configuration in that the partial reflector needs to be placed in between the sample and the objective lens [4-7]. It is critical to overcome this limitation in order to achieve the flexibility of sample positioning in front of the optical probe.

There has been another problem of the fixed path-length difference in a common-path interferometer configuration, especially for the phase-sensitive OCT applications [8-15]. Since the common-path interferometer uses the copropagation of reference and sample beams, it has the advantage of less phase noise compared to the other interferometer

configurations, and thus it is suitable for phase-contrast profile imaging. However, the transverse resolution cannot be reduced below one micrometer because it is difficult to use an objective lens with a high numerical aperture (NA) due to the limited path-length difference between the partial reflector and sample in a conventional common-path interferometer.

In this paper, we report a novel double common-path interferometer configuration that enables the limitless tuning of the objective distance of the sample location. We add an extra duplicate common-path interferometer along the post-path of the interfered optical signal from the original common-path interferometer to generate an interference signal that is independent of the optical distance between the partial reflector and sample.

2. Background

2.1 Limit of Mach-Zehnder interferometer for OCT

Before we investigate the proposed configuration in detail, it is necessary to review the traditional OCT configurations and clarify the limitations of various conventional optical interferometers. Figure 1(a) shows a schematic of the conventional OCT setup based on a Mach-Zehnder interferometer (MZI) and a curled optical fiber probe. When the path-length difference between the sample and reference mirror, $l_S - l_R$, is less than the coherence position of light, the wavelength-swept light source can induce the depth-resolved information of an OCT image. A detailed explanation of the experimental setup will be described later in Section 3. Although the polarization dependence of two optical paths (a sample arm and a reference mirror arm) can affect the OCT image, it has not been a critical issue when a conventional optical cord is used in both arms. However, when a curled optical cord is used in the sample arm as the flexible optical probe, we can clearly see that the OCT image quality varies considerably, depending on the relative polarization state of the two separate arms. Figure 1(b) shows two examples of the OCT image on a fish eye sample generated by tuning the polarization controllers of the two separate arms (one good quality and one poor quality). As the curled optical cord is hanging down freely between the sample and imaging system, the amplitude of the interference signals becomes extremely sensitive to the shape and location of the curled optical cord. Thus, the quality of the OCT image also varies rapidly in real time between good and poor due to the variation in the dynamic range of the signal. Since the logarithm intensity signal of Fig. 1(b) is normalized to the highest peak signal level in each A-scan, the decayed dynamic range is displayed with a vertical strip noise pattern due the enhanced noise level relatively. Otherwise, if the logarithm intensity signal is normalized to the noise signal level, the decayed dynamic range will be displayed with the reduced peak signal in each A-scan. In conclusion of this section, we simply showed the problems in using MZI for a flexible optical probe OCT.

2.2 Limit of conventional common-path interferometer for OCT

Because the MZI is not suitable for the flexible optical probe of OCT, a common-path interferometer has been developed to overcome the polarization mismatch between the reference mirror arm and sample arm of the curled optical cord [3]. Since there is only one path in the common-path interferometer, as shown in Fig. 2(a), the reflected signals from the reference mirror and sample are propagating separately through a commonly shared optical path [4-7]. However, there is still a critical problem with the conventional common-path OCT in that the partial reflector must be located inconveniently close to the sample because the interfered optical signal can be produced only when the delay between the sample arm, l_S, and the reference mirror arm, l_R, is less than the coherence position. Figure 2(b) illustrates an experimental example of this limitation. When the objective distance between the partial reflector and sample, $l_S - l_R$, is 1 mm, the amplitude of the interference signal is

strong enough to obtain the OCT image clearly. As we increase the objective distance to 2 mm and 3 mm by moving the partial reflector position, it is clear that the amplitude of the interference signal is decreased and the quality of the OCT image is proportionally degraded due to the increased sampling frequency and decayed dynamic range of the signal. This result indicates that the flexibility of a curled bending, an arbitrary probe length, and a polarization match can be achieved successfully due to the common-path interferometer; however, the flexibility of the sample position in an optical probe is still a problem that needs to be solved. In conclusion of this section, the conventional common-path interferometer has also the problems for a flexible optical probe OCT. It is critical that we find a method that will enable us to get a good-quality image without requiring us to position the sample close to the partial reflector.

3. Experimental setup

3.1 Setup for double common-path interferometer

Since neither the MZI nor the conventional common-path interferometer is suitable for the flexible optical probe of OCT, we propose a novel configuration for a double common-path interferometer, as shown in Fig. 3(a). To generate an interference signal regardless of the optical distance between the partial reflector and sample, an extra duplicate common-path interferometer can be added along the post-path of the interfered optical signal from the original common-path interferometer. The output of the wavelength-swept laser passes through circulator 1, common-path 1, circulator 2 and common-path 2, in series, and the photodetector. Light from the second port of circulator 1 is partially reflected in order to generate a reference signal (E_R) from the partial reflector 1. The rest of the transmitted light is focused on the sample in order to generate a sample signal (E_S) from each surface of the sample. Assuming a single reflection in the sample, the electric field (E_I) for common-path 1 is represented by

$$
\begin{aligned}
E_1 \quad &= E_R + E_S \\
&= \sqrt{R_R} e^{-j2\frac{\omega}{c} n_F l_R} + \sqrt{R_S} e^{-j2\frac{\omega}{c}\left(n_F l_R + n_A d_1\right)}
\end{aligned}
\tag{1}
$$

where ω ($= 2\pi\nu$) denotes the temporal angular frequency of the light source, n_F and n_A denote the refractive indexes of corresponding media of mainly optical fiber and air, respectively, R_R and R_S denote the reflection coefficients of partial reflector 1 and the sample, respectively, $n_A d_I$ denotes optical path-length difference between the partial reflector and sample, and $n_F l_R$ denotes the common optical distance from circulator 1 to the partial reflector 1.

Common-path 2 induces an additional path-length difference of $2n_A d_2$ to acquire the interference signal in any case in which the objective distance between the partial reflector and sample, $2n_A(l_S - l_R)$ or $2n_A d_I$, is larger than the coherence position, l_C. The signal E_I from common-path 1 enters circulator 2 and common-path 2, in series, and is then reflected by partial reflector 2 and the mirror in common-path 2. Since E_R and E_S are reflected together, four terms (E_{R1}, E_{S1}, E_{R2}, and E_{S2}) are generated in common-path 2. We can represent the electric field (E_2) for common-path 2 as

$$
\begin{aligned}
E_2 \quad &= E_{R1} + E_{S1} + E_{R2} + E_{S2} \\
&= \sqrt{R_R R_P} e^{-j2\frac{\omega}{c}\left(n_F l_R + n_F l_P\right)} + \sqrt{R_S R_P} e^{-j2\frac{\omega}{c}\left(n_F l_R + n_F l_P + n_A d_1\right)} + \sqrt{R_R R_M} e^{-j2\frac{\omega}{c}\left(n_F l_R + n_F l_P + n_A d_2\right)} + \sqrt{R_S R_M} e^{-j2\frac{\omega}{c}\left(n_F l_R + n_F l_P + n_A d_1 + n_A d_2\right)}
\end{aligned}
$$

where R_P and R_M denote the reflection coefficients of partial reflector 2 and the mirror, respectively, and $n_F l_P$ denotes the common optical distance from circulator 2 to partial reflector 2. In the case of tuning the relative path-length difference to $|2n_A(d_1 - d_2)| < l_C$, the

E_{S1} and E_{R2} terms in Eq. (2) can be used to generate an interference fringe. The detected photocurrent I can be expressed as

$$I = \rho \left\langle \left(E_{R1} + E_{S1} + E_{R2} + E_{S2}\right)\left(E_{R1} + E_{S1} + E_{R2} + E_{S2}\right)^{*}\right\rangle \tag{3}$$

where ρ is the responsivity of the detector, and the angular bracket denotes integration over the response time of the detector. In this case, the interference term of the detected photocurrent I can be expressed as

$$I \propto R_R R_S R_P R_M \cos\left(2\frac{\omega}{c} n_A \left(d_1 - d_2\right)\right) \tag{4}$$

This theoretical description implies that an optical distance that is larger than $2n_A d_1$ between a sample and partial reflector 1 in common-path 1 can generate interference successfully by adjusting the extra length of $2n_A d_2$ in common-path 2.

For the generation of an interfered optical signal for the OCT image, we applied a swept-source OCT configuration by using an FDML swept laser with a 2.8 km delayed fiber in the ring cavity to operate at a repetition rate of 71.09 kHz [16]. The tuning range was 102 nm centered at a wavelength of 1295 nm, and the output power was 9 mW. The coherence position (l_C) was around 14.7 mm, which was estimated from the spectral linewidth of 0.05 nm for the laser [17]. The laser output was not filtered or amplified to ensure phase stability. A total of 5% of the laser output propagated to the MZI for resampling the acquired data by interpolating to a uniform spacing in k-space. The MZI generated a comb-like signal corresponding to a frequency shift of 103.3 GHz. The recalibration signal was recorded on the second channel of an A/D converter. The interference signal recorded from the first channel was recalibrated to a frequency shift of the MZI to compensate for the nonlinear frequency sweep of our swept laser. It was then interpolated and fast Fourier transformed to acquire exact phase values [18].

For achieving improved stability for the OCT imaging, same kind of an objective lens and a partial reflector were used in common-paths 1 and 2 because the similar optical beam condition of the objective lens and partial reflector between the two common-paths will reduce the mismatch of length, polarization, and dispersion condition of the interfered optical signal [5]. To reduce environmental vibration, the partial reflector and sample in common-path 1 were mounted on one stage. The partial reflector and mirror in common-path 2 were also mounted on one stage. The partial reflectors in common-paths 1 and 2 consist of a cover glass with two sides. One side, with an antireflection coating, had a reflectivity below 0.002, and the other side had a normal reflectivity of 0.05 in the 1300 ± 50 nm region. For the optimal interference signal, the reflectivity of the partial reflector and mirror could be tuned by an additional surface coating. Since the reduced sensitivity can be caused by the addition of a partial reflector in common-path 2, the analysis of sensitivity is required to provide a quantitative optimization using Eq. (4). Considering the reflectivity of mirror, R_M is 1 in common-path 2, we can obtain the optimally enhanced sensitivity when the reflectivity of the partial reflector R_P in common-path 2 is around 0.33 [4]. By using an additional coated reflector, we expect to enhance the sensitivity of the present method The location of the partial reflector along the focal beam also helped to control the reflected signal intensity from the partial reflector [5].

Depending on the application of OCT, it is sometimes necessary to insert an additional objective lens between the partial reflector and sample in the common-path OCT system. This can be implemented successfully by using the proposed double common-path interferometer. For example, the length of a commercial objective lens body in our

laboratory was measured to be between 28 mm (the lowest NA of 0.1) and 41 mm (the highest NA of 0.85), and thus the path-length difference of $2n_A d_1$ between E_R and E_S is always more than l_C (~14.7 mm) of the wavelength-swept laser light in our OCT system. Therefore, an interference fringe cannot be observed in general when detecting the optical signal of E_1 from common-path 1. To deal with this case, an interferometer with an extra common-path 2 can be useful. This can be achieved by preparing two identical objective lenses and partial reflectors to adjust the path-length difference without limitation, as shown in Fig. 4.

3.2 Phase-sensitive OCT probe with high NA objective lens

To illustrate the usefulness of an arbitrary distance between the sample and partial reflector due to the proposed double common-path interferometer, we demonstrate a phase-sensitive OCT experiment with an enhanced performance achieved by using an objective lens with a high NA over 0.85. This phase-sensitive OCT technology [11] is also known as Spectral Domain Phase Microscopy (SDPM) [12, 13] or Spectral Domain Optical Coherence Phase Microscopy (SD-OCPM) [14]. In order to improve the axial resolutions of OCT below the typical resolution level of a few micrometers, which results from the conventional intensity information of the interference signal, the phase term from the interference signal can be used to measure the sub-coherence-length variations in the axial dimension of the sample. Recently, phase-sensitive OCT has been demonstrated to achieve sub-micrometer axial resolution using the common-path interferometer configuration [11]. Since phase stability is critical for measuring the variation in interference, the common-path interferometer is preferred over other interferometers with separate beam paths, such as the MZI and Michelson interferometer [11-14].

In contrast, the transverse resolution cannot be reduced below one micrometer because it is difficult to use a high-NA objective lens for the conventional common-path interferometer [11-14]. Since, in general, a thin cover glass (thickness 160 μm) should be inserted in the short working distance between the objective lens and sample to serve as a reference reflector, sub-micrometer lateral resolution has not been demonstrated with the common-path configuration because there is a limited space between the sample and high-NA objective lens to insert a cover glass [11-14]. However, in the case of the double common-path configuration, a high-NA objective lens can be positioned near the contact location of the sample successfully by moving the partial reflector far from the sample, as shown in Fig. 4. For improved transverse resolution in phase-sensitive OCT, we used two identical objective lenses (NA = 0.85) for both common-path interferometers. These 0.85-NA objective lenses are the ones with the highest NA in our laboratory, and the focal length is as short as 2.9 mm (working distance = 300 μm; focal depth = 0.4 μm). The theoretical transverse resolution is 1.5 μm for an objective lens with an NA of 0.4, but this can be improved up to 0.7 μm for an objective lens with a high NA of 0.85. If we use a single common-path interferometer by placing a cover glass with a thickness of 160 μm within a working distance of 300 μm, there may be surface damage on the lens or sample and limited control of the reflected signal beam from the partial reflector.

4. Experimental results

Based on the proposed configuration of double common-path OCT, we performed two experiments. The first is the deep OCT imaging independent of the optical distance between the partial reflector and sample using a low-NA objective lens, and the second is the improved transverse-resolution phase-sensitive OCT using a high-NA objective lens.

4.1 Low-NA objective lens probe for deep OCT imaging

Figure 5 shows the cross-sectional images of a fish eye (*Balantiocheilos melanopterus*) acquired at different objective distances between the partial reflector and sample using a double common-path OCT system. The results are compared with those in the case of the previous OCT imaging obtained with the same sample using single common-path OCT, as shown in Fig. 2, where the image quality is degraded due to the dynamic range roll-off as the objective distance increases. In the measurement of Fig. 5, the objective distance between the partial reflector and sample, $l_S - l_R$ or d_1, is increased to 6 mm and 16 mm in common-path 1 only that results in degradation of quality and disappearance of the OCT image, respectively. As we also increase the extra delay distance, d_2, in common-path 2 to move the peak for the point spread function (PSF) toward the 0 mm position of the optical path-length difference, the OCT image can be restored to its original quality, where the sample is near the partial reflector. We can see that the quality of both Figs. 5(a) and 5(b) is similar to that of Fig. 2(b), where $l_S - l_R = 1$ mm. The images consist of 360 axial scans (transverse pixels) with 630 points (axial pixels) per scan. The identical objective lenses used in the measurements of Fig. 2 and Fig. 5 have a low NA of 0.1 for deep OCT imaging. It seems that the dynamic range of double common-path OCT is less than that of Mach-Zehnder- or Michelson-type OCT due to the extra loss term in Eq. (2); however, this configuration has the advantage of enabling a flexible OCT image based on a curled optical cord, as proven by a comparison of the experiment results of Fig. 1 and Fig. 2. Although the extra delay distance, d_2, may be implemented by other interferometers of Mach-Zehnder or Michelson type instead of common-path 2, the common-path interferometer with an identical objective lens has the advantage of enhanced environmental stability [5].

4.2 High-NA objective lens probe for phase-sensitive OCT

The characteristics of a high-NA objective lens, including high transverse resolution, short working distance, and shallow focal depth, enable us to obtain a phase-contrast profile image with a fine structure, which is a good application of phase-sensitive OCT [19]. Before showing the profile measurement for the proposed phase-sensitive OCT configuration, we compare the effect of the transverse resolution of objective lenses with different NA values by using two *en-face* optical coherence microscopy (OCM) images of the USAF 1951 resolution target (group 7), as shown in Figs. 6(a) and 6(b). We selected a small imaging area of group 7 to demonstrate a marginal comparison of transverse resolutions of different NA values. An objective lens with a low NA of 0.4 is used to generate the *en-face* OCM image with a conventional common-path OCT system shown in Fig. 2 because it has a relatively long working distance between the sample and objective lens to insert the partial reflector. In comparison, using the double common-path OCT configuration shown in Fig. 4, two identical objective lenses with an NA of 0.85 are also used to generate the *en-face* OCM image. Since the theoretical transverse resolution is 1.5 μm and 0.7 μm for the objective lenses with an NA of 0.4 and 0.85, respectively, the experimental results clearly show the difference in quality between these two configurations. Figure 6(a) illustrates that a conventional phase-sensitive OCT with of 0.4 NA can marginally distinguish the spacing in element 2 with a somewhat blurred image. In contrast, we can clearly resolve the smallest spacing in element 6 using a double common-path configuration with an objective lens of 0.85 NA, as shown in Fig. 6(b). It is noted that the linewidths of elements 2 and 6 are 3.10 μm and 2.19 μm, respectively. Two axis-translation stages are used to move the sample along the transverse axis under the fixed position of the objective lens in the sample arm. The slight distortion in the OCM image can be improved by tuning the path angle of the translation stage. Though the high NA lens with a short working distance is less convenient to scan along transverse direction, the removal of partial reflector between lens and sample can be an advantage of the proposed double common-path configuration. A pair of Galvano mirrors can replace the translation stage to enhance the imaging speed.

In Figs. 6(c) and 6(d), the phase stability is compared for both the single and double common-path configurations, respectively. For the same light source as for the FDML swept laser, we measured the phase variations in both configurations during 500 axial scans for a mirror sample in a static position. The measured phase variations were converted into time traces of displacement variations. The displacement variations were computed using the relation, where $\delta_z = \lambda_0 \Delta \varphi / 4 \pi n$, where λ_0 is the center wavelength of the light source, and n is the average group index between the partial reflector and mirror sample reflectors [12]. After measuring $\Delta \varphi$ from both configurations during 500 axial scans, the displacement variations were determined. The standard deviations were 505.2 pm and 979.2 pm for the conventional and proposed double common-path configurations, respectively. It appears that the increased phase noise is the result of extra environmental instability and aberration associated with the addition of common-path 2. We expect that the additional instability can be reduced by a shorter length for extra optic components and the replacement of the circulator with a directional coupler. Nevertheless, it is a more critical advantage that the double common-path interferometer can enhance the transverse resolution due to the use of a higher-NA objective lens and can support the flexibility of the sample position from the objective lens. Even with the increased displacement variation, the system can measure a nanometer-scale axial-displacement profile.

Figure 7 shows nanometer-scale 3D phase-contrast profile images that were obtained using a double common-path phase-sensitive OCT configuration with an objective lens with a high NA of 0.85. For a sample of the USAF 1951 resolution target, the 3D OCT data set, consisting of $1024 \times 512 \times 1000$ voxels, is recorded for both the *en-face* OCM images and the phase-profile images. The intensity profile (Fig. 6(b)) and phase profile (Figs. 7(a) and 7(b)) are imaged from one data set measurement. The measurement of the phase variation corresponds to the sub-coherence-length variation in the selected sample layer given by the simple relation $\delta_z = \lambda_0 \Delta \varphi / 4 \pi n$, where λ_0 is the center wavelength of the light source, $\Delta \varphi$ is the unwrapped phase variation, and n is the refractive index between the partial reflector and sample [12]. The converted height profile of the patterned chromium layer has a nanometer-scale axial resolution. By using a high-NA objective lens, the spacings of the smallest elements can also be clearly resolved with sub-micrometer transverse resolution.

To demonstrate potential industry applications, we repeated the experiment using a hologram pattern on a photoresist substrate. A positive photoresist substrate (AZ 151) was exposed to UV light in order to create holes that were 2 µm in diameter and 200 nm in depth. This sample was an intermediate product before electroforming. From the 3D surface profile images of Figs. 7(c) and 7(d), small variations within the sub-coherence length, such as hole depth, cone shape symmetry, and surface debris defects, can be clearly monitored with high axial and transverse resolutions. Figure 7(c) was imaged from a 3D data set of $1024 \times 500 \times 500$ voxels. The entire 3D data were acquired by recording each 2D data set in sequence on a computer system memory. This 3D imaging information is useful to check for a match with the designed parameters and to provide feedback to optimize the fabrication process in real time. Using the phase-sensitive OCT system, it was impossible to measure the same sample with a similar axial and lateral resolution simultaneously. When the same sample was measured by atomic force microscopy (AFM), it was difficult to get an exact profile because the sample surface was damaged by the physical contact of the AFM probe tip with the target.

5. Conclusion

In summary, we demonstrated a novel OCT system based on a double common-path interferometer that enables flexible curled bending, arbitrary probe length, and probe-sample separation. Our proposed configuration enhanced the convenience of sample position in

common-path interferometer, like the other Michelson and Mach-Zehnder interferometers. By adjusting the additional delay time by the second common-path interferometer, the optical path-length difference of sample position can be moved to near the zero-delay position where high dynamic range is obtained by lowering the sampling frequency. In addition, with the all-fiber double common-path configuration, the phase noise can be reduced so that our system can be applied to the phase-sensitive OCT imaging with high transverse resolution. We obtained simultaneously a high axial-resolution imaging with nanometer-scale phase stability and a high transverse-resolution imaging with sub-micrometer resolving power using a phase-sensitive OCT configuration with two identical high-NA objective lenses. We expect that the 3D surface profile image will be more practical for the in-line product inspection of fine-structure samples and for *in vivo* endoscopic imaging of biomedical samples.

Acknowledgments

References and links

1. Huang D, Swanson EA, Lin CP, Schuman JS, Stinson WG, Chang W, Hee MR, Flotte T, Gregory K, Puliafito CA, Fujimoto J. Optical coherence tomography. Science. 1991; 254(5035):1178–1181. [PubMed: 1957169]

2. Youngquist RC, Carr S, Davies DEN. Optical coherence-domain reflectometry: a new optical evaluation technique. Opt. Lett. 1987; 12(3):158–160. [PubMed: 19738824]

3. Park JS, Jeong MY, Jung CH, Ouh CH, Kang HJ, Han YG, Lee SB, Kim CS. Flexible curled optical cord for bending-insensitive optical imaging delivery. IEEE J. Sel. Top. Quantum Electron. 2010; 16(4):1031–1038.

4. Sharma U, Fried NM, Kang JU. All-fiber common-path optical coherence tomography: sensitivity optimization and system analysis. IEEE J. Sel. Top. Quantum Electron. 2005; 11(4):799–805.

5. Park JS, Jeong MY, Kim CS. Post-tuning of sample position in common-path swept source optical coherence tomography. J. Opt. Soc. Korea. 2011; 15 to be published.

6. Vakhtin AB, Kane DJ, Wood WR, Peterson KA. Common-path interferometer for frequency-domain optical coherence tomography. Appl. Opt. 2003; 42(34):6953–6958. [PubMed: 14661810]

7. Tumlinson AR, Barton JK, Povazay B, Sattman H, Unterhuber A, Leitgeb RA, Drexler W. Endoscope-tip interferometer for ultrahigh resolution frequency domain optical coherence tomography in mouse colon. Opt. Express. 2006; 14(5):1878–1887. [PubMed: 19503517]

8. Izatt JA, Kulkarni MD, Wang HW, Kobayashi K, Sivak MV. Optical coherence tomography and microscopy in gastrointestinal tissues. IEEE J. Sel. Top. Quantum Electron. 1996; 2(4):1017–1028.

9. Huang SW, Aguirre AD, Huber RA, Adler DC, Fujimoto JG. Swept source optical coherence microscopy using a Fourier domain mode-locked laser. Opt. Express. 2007; 15(10):6210–6217. [PubMed: 19546926]

10. Lee JH, Jung EJ, Kim CS. Optical coherence tomography based on a continuous wave supercontinuum seeded by erbium doped fiber's amplified spontaneous emission. J. Opt. Soc. Korea. 2010; 14(1):49–54.

11. Adler DC, Huber R, Fujimoto JG. Phase-sensitive optical coherence tomography at up to 370,000 lines per second using buffered Fourier domain mode-locked lasers. Opt. Lett. 2007; 32(6):626–628. [PubMed: 17308582]

12. Zhang J, Rao B, Yu L, Chen Z. High-dynamic-range quantitative phase imaging with spectral domain phase microscopy. Opt. Lett. 2009; 34(21):3442–3444. [PubMed: 19881621]

13. Choma MA, Ellerbee AK, Yang C, Creazzo TL, Izatt JA. Spectral-domain phase microscopy. Opt. Lett. 2005; 30(10):1162–1164. [PubMed: 15945141]

14. Joo C, Akkin T, Cense B, Park BH, de Boer JF. Spectral-domain optical coherence phase microscopy for quantitative phase-contrast imaging. Opt. Lett. 2005; 30(16):2131–2133. [PubMed: 16127933]

15. Endo T, Yasuno Y, Makita S, Itoh M, Yatagai T. Profilometry with line-field Fourier-domain interferometry. Opt. Express. 2005; 13(3):695–701. [PubMed: 19494930]

16. Huber R, Wojtkowski M, Fujimoto JG. Fourier Domain Mode Locking (FDML): A new laser operating regime and applications for optical coherence tomography. Opt. Express. 2006; 14(8): 3225–3237. [PubMed: 19516464]

17. Yun, SH.; Bouma, BE. Wavelength swept lasers. In: Drexler, W.; Fujimoto, JG., editors. Optical Coherence Tomography: Technology and Applications. Springer: 2008.

18. Yun SH, Tearney GJ, de Boer JF, Bouma BE. Removing the depth-degeneracy in optical frequency domain imaging with frequency shifting. Opt. Express. 2004; 12(20):4822–4828. [PubMed: 19484034]

19. Kim D, Cho YJ. 3-Dsurface profile measurement using an acousto optic tunable filter based spectral phase shifting technique. J. Opt. Soc. Korea. 2008; 12(4):281–287.
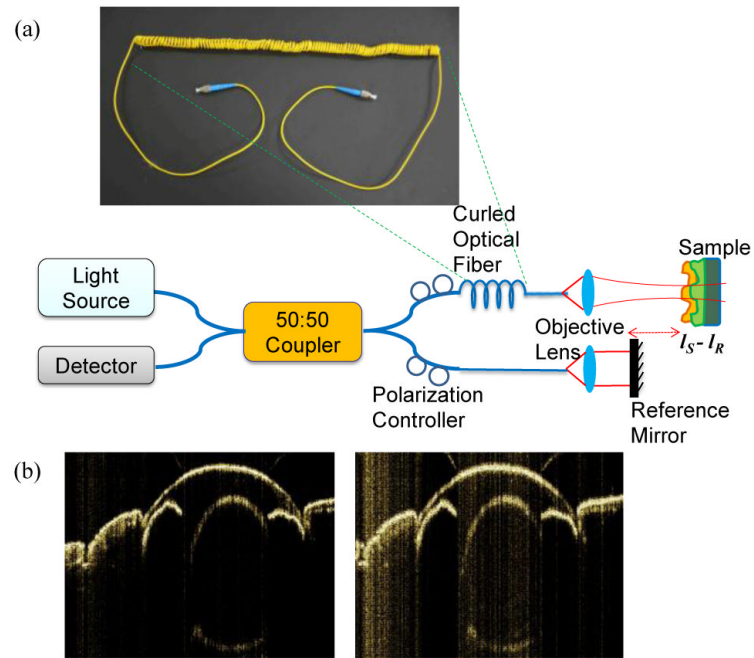
Fig. 1.
(a) Schematic of the conventional OCT setup based on a Mach-Zehnder interferometer and a curled optical fiber probe. (b) Variation of OCT image quality depending on the polarization state by tuning polarization controllers.
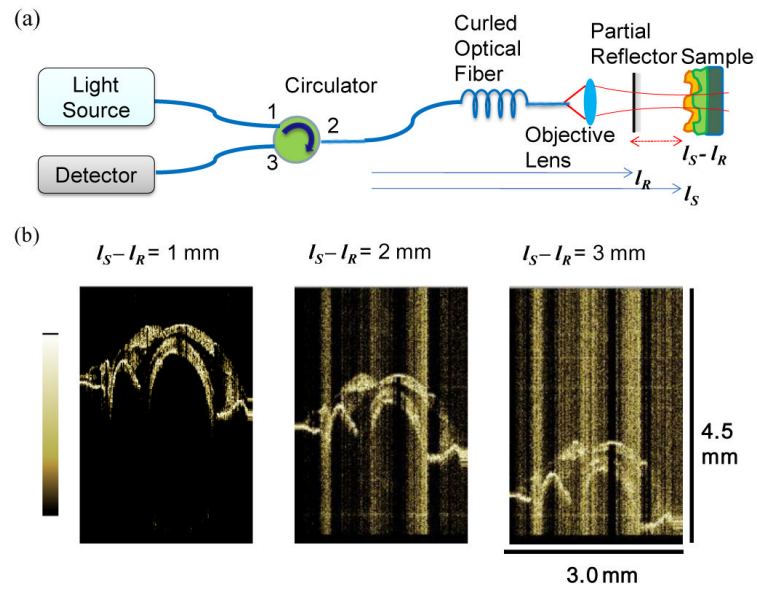
Fig. 2.
(a) Schematic of the conventional OCT setup based on a conventional common-path interferometer and a curled optical fiber probe. (b) Variation of OCT image quality depending on the objective distance by moving the position of the partial reflector.
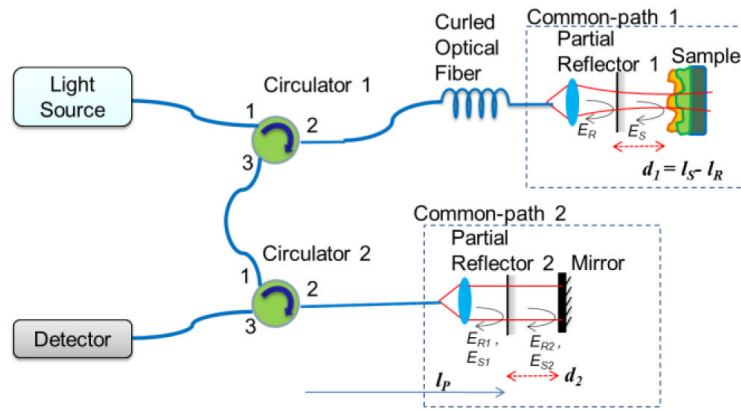
Fig. 3.
Schematic of the proposed double common-path OCT setup.
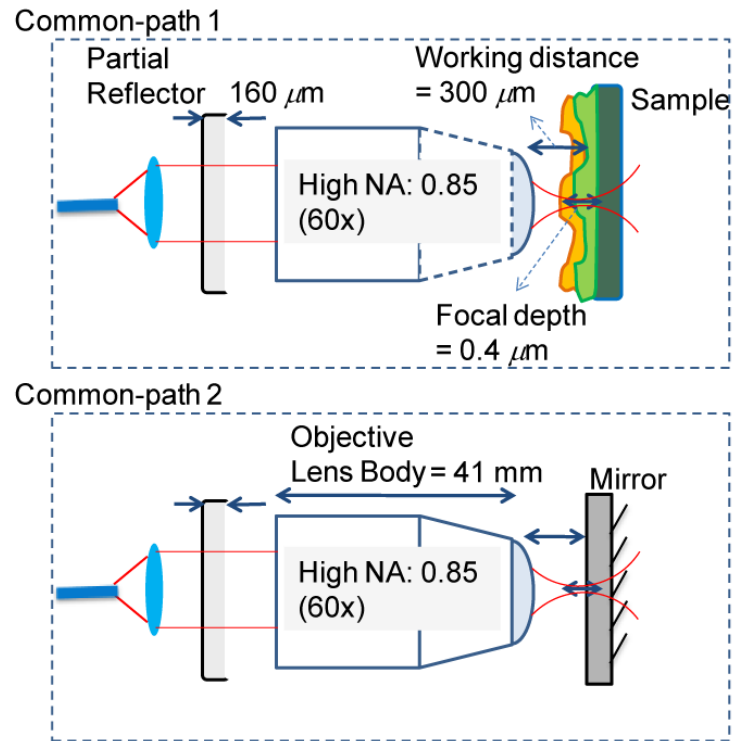
Fig. 4.
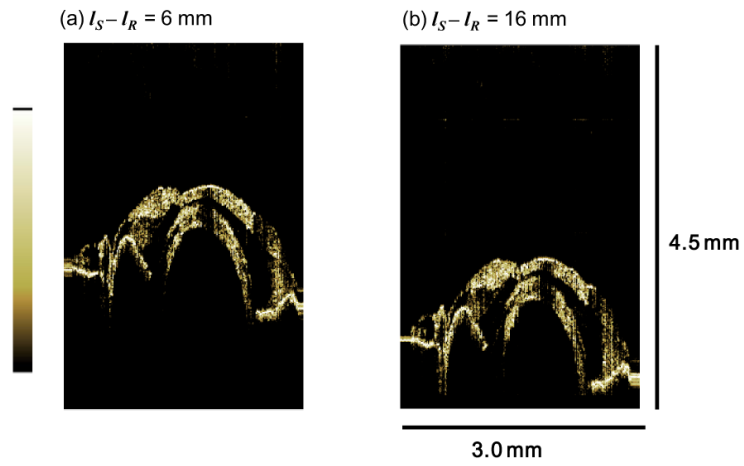Schematic of a phase-sensitive OCT probe based on the double common-path interferometer setup, as shown in Fig. 3.

Fig. 5.
Maintaining OCT image quality for different objective distances of (a) 6 mm and (b) 16 mm, respectively, using the proposed double common-path OCT system with a low NA objective lens (NA = 0.1).
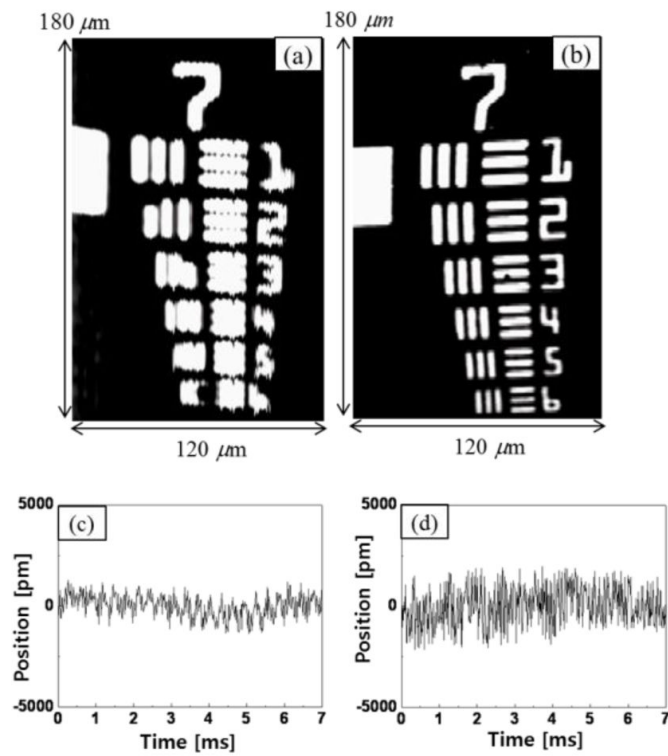
Fig. 6.
Conventional phase-sensitive OCT (NA = 0.4) measures (a) *en-face* OCM image and (c) time trace of displacement; double common-path phase-sensitive OCT (NA = 0.85) measures (b) *en-face* OCM image and (d) time trace of displacement.
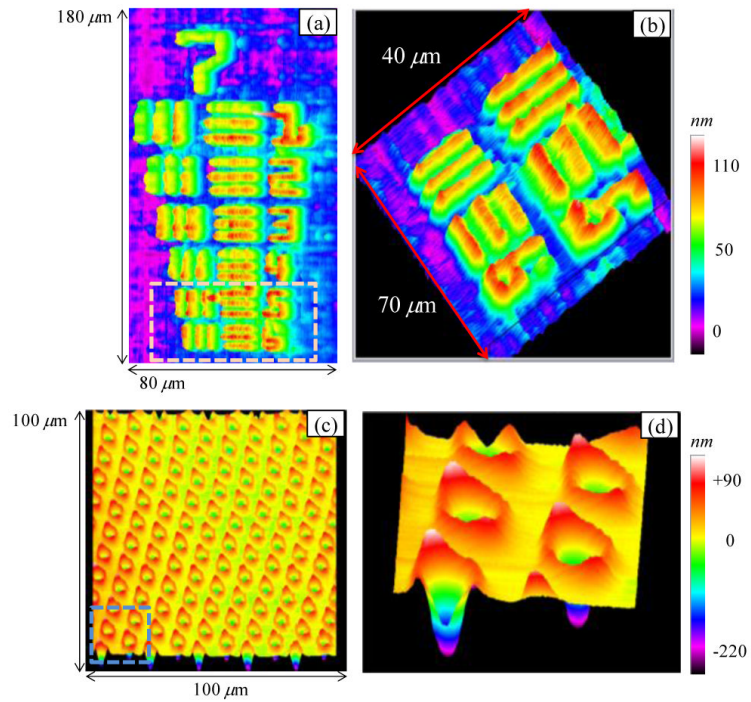
Fig. 7.
3D phase-contrast surface profile images of (a) group 7, (b) enlargement of elements 5, 6 of the USAF 1951 resolution target, (c) a hologram pattern with $100 \times 100 \ \mu m^2$ area, and (d) enlargement of the marked region ($20 \times 20 \ \mu m^2$).